The intestinal stem cell markers Bmi1 and Lgr5 identify two functionally distinct populations

Kelley S. Yan[a], Luis A. Chia[a], Xingnan Li[a], Akifumi Ootani[a], James Su[b], Josephine Y. Lee[c], Nan Su[d], Yuling Luo[d], Sarah C. Heilshorn[b], Manuel R. Amieva[c,e], Eugenio Sangiorgi[f], Mario R. Capecchi[g,1], and Calvin J. Kuo[a,1]

Departments of [a]Medicine, [b]Materials Science and Engineering, [c]Microbiology and Immunology, and [e]Pediatrics, Stanford University School of Medicine, Stanford, CA 94305; [d]Advanced Cell Diagnostics, Inc., Hayward, CA 94545; [f]Istituto di Genetica Medica, Università Cattolica del Sacro Cuore, 00168 Rome, Italy; and [g]Howard Hughes Medical Institute and Department of Human Genetics, University of Utah School of Medicine, Salt Lake City, UT 84112

Contributed by Mario R. Capecchi, November 21, 2011 (sent for review October 28, 2011)

The small intestine epithelium undergoes rapid and continuous regeneration supported by crypt intestinal stem cells (ISCs). Bmi1 and Lgr5 have been independently identified to mark long-lived multipotent ISCs by lineage tracing in mice; however, the functional distinctions between these two populations remain undefined. Here, we demonstrate that Bmi1 and Lgr5 mark two functionally distinct ISCs in vivo. Lgr5 marks mitotically active ISCs that exhibit exquisite sensitivity to canonical Wnt modulation, contribute robustly to homeostatic regeneration, and are quantitatively ablated by irradiation. In contrast, Bmi1 marks quiescent ISCs that are insensitive to Wnt perturbations, contribute weakly to homeostatic regeneration, and are resistant to high-dose radiation injury. After irradiation, however, the normally quiescent Bmi1$^+$ ISCs dramatically proliferate to clonally repopulate multiple contiguous crypts and villi. Clonogenic culture of isolated single Bmi1$^+$ ISCs yields long-lived self-renewing spheroids of intestinal epithelium that produce Lgr5-expressing cells, thereby establishing a lineage relationship between these two populations in vitro. Taken together, these data provide direct evidence that Bmi1 marks quiescent, injury-inducible reserve ISCs that exhibit striking functional distinctions from Lgr5$^+$ ISCs and support a model whereby distinct ISC populations facilitate homeostatic vs. injury-induced regeneration.

R-spondin | Dickkopf-1 | intestinal regeneration

The G protein-coupled receptor Lgr5 and the Polycomb group protein Bmi1 are two recently described molecular markers of self-renewing and multipotent adult stem cell populations residing in the crypt of the small intestine, capable of supporting regeneration of the intestinal epithelium (1, 2). Despite their similar ability to functionally repopulate the intestinal epithelium as demonstrated by independent in vivo lineage tracing experiments in reporter mice, the intestinal stem cells (ISCs) identified by these two molecular markers are spatially distinct. Whereas Lgr5$^+$ ISCs are crypt base columnar (CBC) cells (1, 3) interspersed between Paneth cells and expressed throughout the intestine, Bmi1$^+$ ISCs are mostly restricted to the "+4" cell position abutting the uppermost Paneth cell in proximal small intestine crypts (2). Lgr5$^+$ ISCs are actively cycling (1), equipotent, and contribute to intestinal homeostasis by neutral drift competition (4–6). By comparison, Bmi1$^+$ ISCs are less well characterized, and because of the lack of direct evidence, their cell cycle status is variably ascribed to be rapidly (7) vs. slowly cycling (8). It has been suggested that Bmi1 and Lgr5 mark an overlapping and possibly identical or redundant population of ISCs (5, 7, 9); however, no direct exploration of their functional similarities and differences has been performed. Further, it is unknown how Bmi1$^+$ and Lgr5$^+$ ISCs relate to a proposed model in which the intestine differentially uses an actively cycling ISC population during homeostasis and a distinct quiescent, injury-induced ISC population (10, 11) during epithelial repair. We therefore conducted a systematic comparison of Bmi1$^+$ and Lgr5$^+$ ISC function during homeostasis and injury repair to investigate whether Lgr5 and Bmi1 mark identical, similar, or distinct ISC populations.

Results

Bmi1 Marks Quiescent ISCs That Contribute Minimally to Intestinal Homeostasis. Given the spatial localization of Bmi1$^+$ ISCs at the +4 position, where a DNA label-retaining cell has also been described (12, 13), we postulated that Bmi1 marks a quiescent ISC. Lgr5-eGFP-IRES-CreERT2 and Bmi1-CreER; Rosa26-YFP mice were used to compare the basal proliferation status of Lgr5$^+$ vs. Bmi1$^+$ ISCs during homeostasis. We used short-term tamoxifen exposure, for induction of Cre-mediated recombination, to selectively mark Bmi1$^+$ ISCs in vivo. Accordingly, Bmi1-CreER; Rosa26-YFP mice were treated with tamoxifen 1–2 d before killing to genetically label Bmi1$^+$ cells with YFP, revealing one to two YFP$^+$ cells at approximately the +4 cell position (ranging from +1 to +6) within ≈10% of proximal small intestine crypts, in agreement with previous reports (2). To determine basal proliferation status, labeling of actively cycling S phase cells was performed by using the thymidine analog 5-ethynyl-2′-deoxyuridine (EdU). Under steady-state conditions, histological examination of small intestine revealed 31 ± 5.2% EdU incorporation among Lgr5$^+$ ISCs, identified as GFP$^+$ CBC cells in Lgr5-eGFP-IRES-CreERT2 mice. In contrast, only 1.7 ± 0.30% of Bmi1$^+$ ISCs, identified by the crypt Rosa-YFP$^+$ signal after 1.5-d tamoxifen exposure in Bmi1-CreER; Rosa26-YFP mice, incorporated EdU (Fig. 1 *A–F* and *N*).

To examine the relative contribution of Lgr5 vs. Bmi1 ISCs to tissue regeneration under steady-state conditions, lineage tracing was induced by tamoxifen administration in Cre reporter mice to mark the ISCs and their respective progeny. Upon tamoxifen-mediated lineage tracing of Lgr5$^+$ and Bmi1$^+$ ISCs in Lgr5-eGFP-IRES-CreERT2; Rosa26-TdTomato and Bmi1-CreER; Rosa26-YFP mice, Lgr5$^+$ ISCs were markedly more efficient at generating progeny than Bmi1$^+$ ISCs by 7 d of lineage tracing with 95 ± 1.7% vs. 18 ± 5.1% lineage "stripe" generation, respectively (Fig. 1 *G–I*). This method also likely underestimates their substantial relative difference in progeny generation because of the more qualitatively vigorous nature of Lgr5 striping. Overall, these differences in basal proliferation and lineage-forming efficiency reflect a much greater functional contribution of Lgr5$^+$ ISCs to homeostatic small intestine regeneration compared with Bmi1$^+$ ISCs.

Author contributions: K.S.Y., Y.L., S.C.H., M.R.A., E.S., M.R.C., and C.J.K. designed research; K.S.Y., L.A.C., X.L., A.O., J.S., J.Y.L., and N.S. performed research; E.S. and M.R.C. contributed new reagents/analytic tools; K.S.Y., L.A.C., X.L., A.O., J.S., and C.J.K. analyzed data; and K.S.Y. and C.J.K. wrote the paper.

The authors declare no conflict of interest.

Freely available online through the PNAS open access option.

[1]To whom correspondence may be addressed. E-mail: cjkuo@stanford.edu or mario.capecchi@genetics.utah.edu.

This article contains supporting information online at www.pnas.org/lookup/suppl/doi:10.1073/pnas.1118857109/-/DCSupplemental.

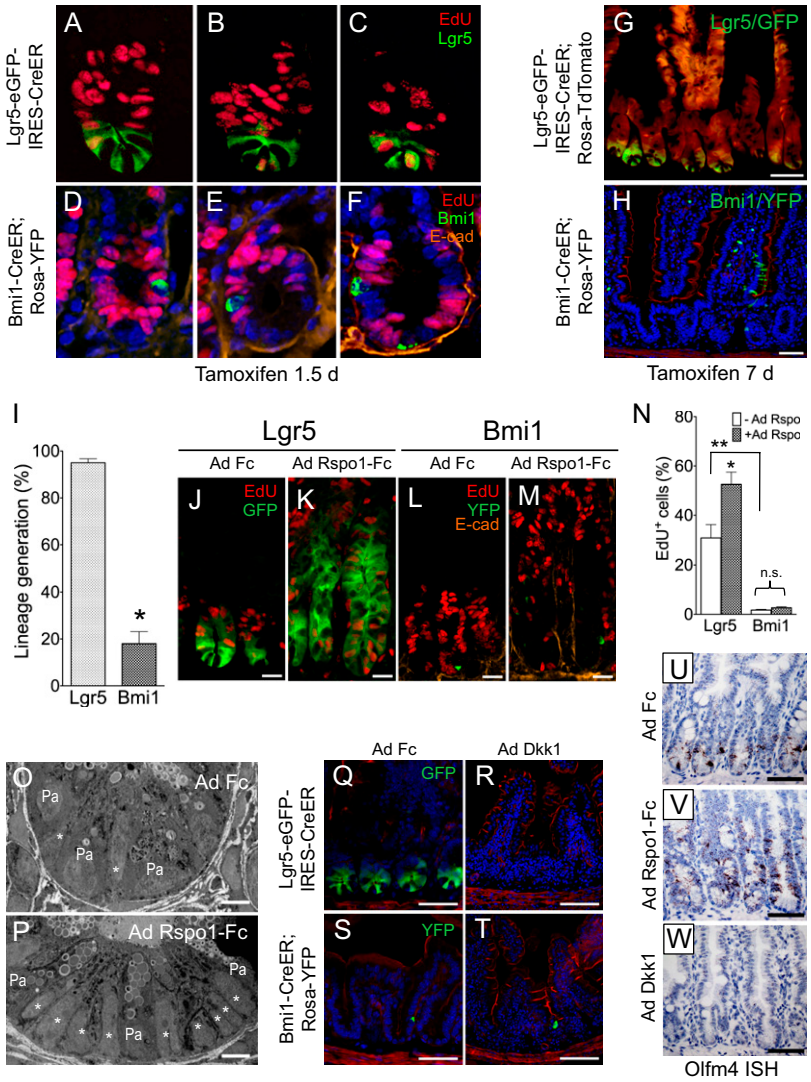

Fig. 1. Basal proliferation status and response to canonical Wnt pathway modulation of Lgr5$^+$ vs. Bmi1$^+$ ISCs. (*A–F* and *N*) Lgr5-eGFP$^+$ ISCs in Lgr5-eGFP-IRES-CreERT2 duodenum are actively cycling and incorporate EdU under homeostasis (*A–C*). In contrast, Bmi1$^+$ ISCs labeled with 1.5-d tamoxifen exposure in Bmi1-CreER; Rosa26-YFP duodenum are slowly cycling and do not incorporate EdU (*D–F*, $^{**}P = 0.0049$ vs. Lgr5; DAPI colored in blue). (*G–I*) Lgr5$^+$ ISCs in Lgr5-eGFP-IRES-CreERT2; Rosa26-TdTomato duodenum generate progeny much more efficiently than Bmi1$^+$ ISCs in Bmi1-CreER; Rosa26-YFP duodenum by 7 d after tamoxifen-mediated lineage tracing ($^*P = 0.0001$). TdTomato is shown in red (*G*); phalloidin is colored in red and DAPI in blue (*H*). (*J–N*) Consequences of canonical Wnt stimulation with Ad Rspo1-Fc on Lgr5$^+$ vs. Bmi1$^+$ ISCs. Marked expansion of Lgr5-eGFP$^+$ ISCs and the transit-amplifying compartment are seen by direct fluorescence microscopy, whereas Bmi1-YFP$^+$ ISCs are less responsive to Ad Rspo1-Fc stimulation. Notably, Ad Rspo1-Fc results in enhanced EdU incorporation in Lgr5-eGFP$^+$ ISCs ($^*P = 0.04$) but not in Bmi1-YFP$^+$ ISCs ($P = 0.13$) compared with Ad Fc control. (*O* and *P*) Electron microscopy reveals expansion of crypt base columnar (CBC) cells (*) consistent with Lgr5$^+$ ISC morphology in between Paneth cells (Pa) after Ad Rspo1-Fc treatment. (*Q* and *R*) Canonical Wnt inhibition with Ad Dkk1 results in complete loss of Lgr5-eGFP$^+$ ISCs. (*S* and *T*) In contrast, Bmi1-YFP$^+$ cells persist despite systemic Wnt blockade with Ad Dkk1. (*Q–T*) Phalloidin is colored in red and DAPI in blue. (*U–W*) In situ hybridization (ISH) analysis reveals enhanced expression of Olfm4, a surrogate marker for Lgr5, in response to Ad Rspo1-Fc stimulation of canonical Wnt signaling (*V*), whereas Ad Dkk1 results in complete loss of Olfm4 expression (*W*) compared with Ad Fc control (*U*). (Scale bars: *H*, *Q–W*, 50 μm; *J–M*, 20 μm; *O* and *P*, 5 μm.)

Differential Responses of Bmi1$^+$ vs. Lgr5$^+$ ISCs to Canonical Wnt Modulation. Because Lgr5$^+$ and Bmi1$^+$ ISCs reside in spatially distinct crypt locations, we explored whether they exhibited differential responses to global modulation of the canonical Wnt pathway, which is required to maintain adult intestine epithelial proliferation and crypt architecture (14–16). Gain- and loss-of-function manipulation of the canonical Wnt signaling pathway was achieved in mice by using adenoviral expression of the soluble, secreted factors R-Spondin1 (Rspo1) (17, 18) and Dickkopf-1 (Dkk1) (14), respectively. A single i.v. injection of adenovirus encoding either the Wnt agonist Rspo1 or antagonist Dkk1 results in hepatic infection and transduction, secretion of the recombinant factor into the systemic circulation, and leads to profound histological changes in the intestinal epithelium within 5 d after infection (14). In Lgr5-eGFP-IRES-CreERT2 and Bmi1-CreER; Rosa26-YFP mice, canonical Wnt signaling was potently induced by systemic administration of an adenovirus encoding Rspo1 fused to an IgG2α Fc fragment (Ad Rspo1-Fc), causing marked crypt hypertrophy and hyperproliferation. By 5 d after infection, Ad Rspo1-Fc markedly expanded Lgr5-eGFP$^+$ cells, and expression of the surrogate marker Olfm4 (7), which was not seen with a control adenovirus encoding IgG2α Fc (Ad Fc) (Fig. 1 *J*, *K*, *U*, and *V* and Fig. S1 *A* and *B*). Electron microscopy of Ad Rspo1-Fc–treated small intestine confirmed expansion of multiple consecutive slender CBC cells between Paneth cells, consistent with substantially increased numbers of

Lgr5$^+$ ISCs, compared with only single CBC cells between Paneth cells with Ad Fc treatment (Fig. 1 *O* and *P*). In contrast, Ad Rspo1-Fc treatment did not significantly alter either the relative abundance or the mitotic index of Bmi1$^+$ ISCs labeled with 1- or 2-d tamoxifen exposure in Bmi1-CreER; Rosa26-YFP mice (Fig. 1 *L–N* and Fig. S1 *D* and *E*). Further, Ad Rspo1-Fc did not enhance the basal level of infrequent lineage stripes arising from Bmi1$^+$ ISCs despite dramatic concurrent expansion of the crypt compartment (Fig. S1 *G–I*) and Lgr5-eGFP$^+$ cells (Fig. 1*K*).

Conversely, systemic Wnt loss-of-function studies were performed in these reporter mice by using adenovirus encoding Dkk1 (Ad Dkk1), which has been reported to induce rapid crypt loss and destruction of the small intestine epithelial architecture (14) (Fig. 1 *Q–T*). Correspondingly, Ad Dkk1 induced a profound loss of Lgr5-eGFP and Olfm4 expression in the small intestine crypts (Fig. 1 *Q*, *R*, *U*, and *W* and Fig. S1 *A* and *C*). In contrast to the dramatic effect on Lgr5$^+$ ISCs, Ad Dkk1 treatment did not significantly diminish 1- or 2-d tamoxifen-labeled Bmi1$^+$ ISCs in Bmi1-CreER; Rosa26-YFP mice, which, in fact, persisted despite Ad Dkk1-mediated crypt loss (Fig. 1 *S* and *T* and Fig. S1 *D* and *F*). Thus, the Lgr5-eGFP$^+$ but not the Bmi1$^+$ ISC population exhibited exquisite sensitivity to global gain- and loss-of-function Wnt signaling modulation mediated by Rspo1 and Dkk1, respectively, highlighting substantial functional differences between the response of these two ISC populations to extracellular Wnt signals.

Differential Responses of Bmi1$^+$ vs. Lgr5$^+$ ISCs to Radiation Injury. We further probed the functional differences between Lgr5$^+$ and Bmi1$^+$ ISCs by using a radiation injury model. Lgr5-eGFP-IRES-CreERT2 and Bmi1-CreER; Rosa26-YFP mice were treated with 12 Gy whole-body irradiation. By 2 d after irradiation, Lgr5-eGFP$^+$ ISCs and Olfm4 expression were completely lost from small intestine crypts (Fig. 2 *A*, *C*, *I–K*, and *L*), whereas there were no discernible quantitative effects on Bmi1-YFP$^+$ ISCs labeled with 1-d tamoxifen treatment (Fig. 2 *B* and *D*). By 4.5 and 7 d after irradiation, rare Lgr5-eGFP$^+$ cells reemerged, scattered sporadically throughout the small intestine at a frequency of ≈1/180 total crypts, but these were still severely diminished compared with unirradiated littermate controls (Fig. 2 *E* and *G*). In contrast, irradiation induced a strong proliferative response in 1-d tamoxifen-treated Bmi1$^+$ ISCs, 17 ± 1.5% of which were robustly labeled with EdU by 2 d after irradiation, compared with 1.7 ± 0.30% during homeostasis (Fig. 2 *O–R*); this increased proliferation was accompanied by a fivefold expansion in Bmi1-YFP$^+$ ISCs/progeny upon fluorescence activated cell sorting (FACS) analysis by 4.5 d after irradiation vs. unirradiated littermate controls (Fig. 2 *M* and *N*).

We also examined the functional effects of irradiation on the ability of Lgr5$^+$ vs. Bmi1$^+$ ISCs to generate downstream progeny. Two serial tamoxifen injections in Lgr5-eGFP-IRES-CreERT2; Rosa26-YFP mice, 1 d before and 1 d after irradiation, were used to irreversibly mark the Lgr5$^+$ lineage with YFP, in a manner independent of concurrent Lgr5 expression. Accordingly, both YFP-marked Lgr5$^+$ cells and their downstream progeny were eradicated by 4.5 and 7 d after irradiation (Fig. 3 *A* and *B*). Similarly, a single tamoxifen injection in Bmi1-CreER; Rosa26-YFP mice was used to irreversibly mark the Bmi1$^+$ lineage, followed 2 d later by 12 Gy irradiation and tissue harvest at 7 d after irradiation. As opposed to the quantitative eradication of Lgr5$^+$ ISC-derived progeny, irradiation substantially induced expansion of the Bmi1$^+$ lineage. Indeed, by 7 d after irradiation in regenerating small intestine, confluent Bmi1$^+$ ISC-derived YFP$^+$ lineage stripes were seen along multiple adjacent crypts and villi, which were much more extensive than the comparatively atretic Bmi1$^+$ lineage tracing present during homeostasis (Fig. 3 *C* and *D* and Fig. S2).

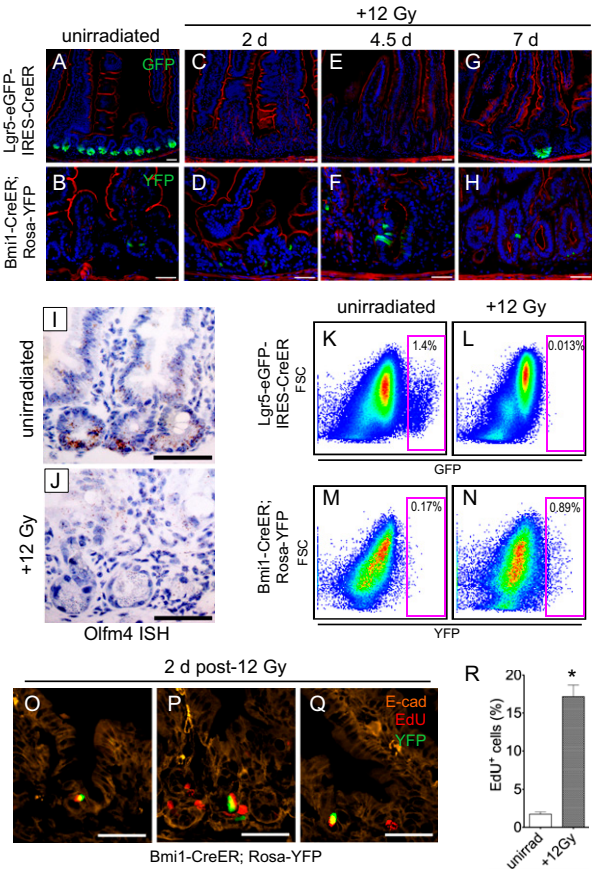

Fig. 2. Differential responses of Lgr5$^+$ vs. Bmi1$^+$ ISCs to acute radiation injury. (*A–H*) Direct fluorescence detection of Lgr5-eGFP$^+$ vs. Bmi1-YFP$^+$ ISCs. Phalloidin is depicted in red and DAPI in blue. (*A* and *B*) Unirradiated duodenum with Lgr5-eGFP$^+$ cells in the crypt bases and rare Bmi1-YFP$^+$ ISCs labeled with 1-d tamoxifen exposure in Bmi1-CreER; Rosa-YFP mice. (*C–F*) Lgr5-eGFP$^+$ ISCs are completely lost (*C* and *E*), whereas Bmi1-YFP$^+$ ISCs (*D* and *F*) persist by 2 and 4.5 d after 12 Gy whole-body irradiation. (*G* and *H*) Lgr5-eGFP$^+$ ISCs return in sporadic (≈1/180) crypt bases (*G*) and Bmi-YFP$^+$ ISCs are quantitatively unchanged by 7 d after 12 Gy whole-body irradiation (*H*). (*I* and *J*) Olfm4 ISH demonstrates loss of Olfm4 expression in crypt bases by 2 d after 12 Gy irradiation confirming loss of Lgr5 expression. (*K–N*) FACS analysis demonstrates loss of Lgr5-eGFP$^+$ epithelial cells by 2 d (*K* and *L*), in contrast to expansion of Bmi1-YFP$^+$ cells/progeny by 4.5 d after 12 Gy whole-body irradiation (*M* and *N*). (*O–R*) Enhanced proliferation of Bmi1-YFP$^+$ ISCs by 2 d after 12 Gy irradiation revealed by EdU incorporation (*P = 0.0006, n = 3 mice, unpaired Student's t test). (Scale bars: 50 μm.)

Strikingly, the Bmi1$^+$ lineage showed postirradiation extension into multiple adjacent crypts and villi emanating from a single crypt as revealed by three-dimensional (3D) confocal reconstruction (Fig. 3 *E–G* and Movie S1). We also treated Bmi1-CreER; Rosa26-Confetti mice with tamoxifen 2 d before 12 Gy irradiation to stochastically label individual Bmi1$^+$ ISCs with one of four possible fluorescent colors (4) and trace their fate in response to injury. Using this multicolor reporter to visualize the dramatic expansion of the Bmi1$^+$ lineage, the progeny arising from the marked clones were noted to be exclusively labeled with a single color at 7 d after irradiation, attesting to their monoclonal origin despite their extension into contiguous crypts and villi (Fig. 3 *H–K* and Movie S2). Thus, compared with the radiosensitive, actively cycling Lgr5-eGFP$^+$ ISCs, the quiescent Bmi1$^+$ ISCs exhibit radioresistance and are rapidly mobilized to proliferate upon injury with significant contribution to epithelial regeneration, and pronounced induction of Bmi1$^+$ lineage tracing. Taken together, these data suggest that Bmi1$^+$ ISCs are quiescent

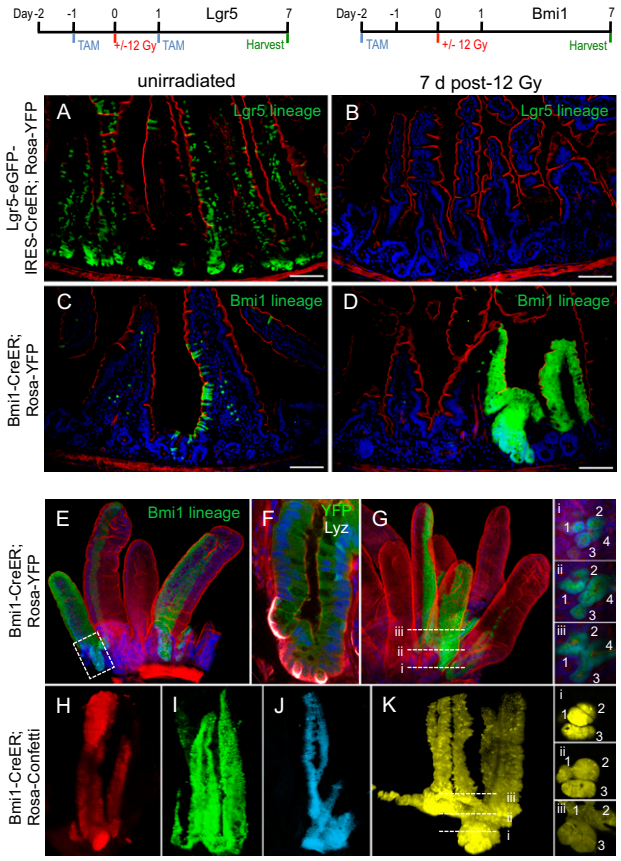

Fig. 3. Differential responses of Lgr5$^+$ vs. Bmi1$^+$ lineages to acute radiation injury. (*A* and *B*) Tamoxifen-mediated lineage trace of Lgr5-eGFP$^+$ progeny in Lgr5-eGFP-IRES-CreERT2; Rosa-YFP mouse duodenum demonstrates prolific lineage generation under homeostasis by 8 d (*A*). Lgr5-eGFP$^+$ ISCs and their lineage are ablated at 7 d after 12 Gy whole-body irradiation (*B*). (*C* and *D*) Bmi1$^+$ lineage in Bmi1-CreER; Rosa-YFP duodenum marked by 9-d tamoxifen treatment exhibits marked proliferative regenerative response with progeny observed in adjacent crypts and villi at 7 d after irradiation. (Scale bars; *A–D*, 100 μm.) Phalloidin is shown in red and DAPI in blue. (*E–G*) 3D confocal reconstruction of Bmi1$^+$ lineage regenerative response in the jejunum at 7 d after 12 Gy irradiaton highlights confluent patches of Bmi1$^+$-derived cells in multiple adjacent crypts/villi. Zoomed view of regenerated jejunum immunostained with lysozyme, illustrating Paneth cells within a budding crypt (*F*). Phalloidin is colored in red and DAPI in blue. (*H–K*) Monoclonal repopulation of 7 d postirradiated jejunum from Bmi1-CreER; Rosa-Confetti compound heterozygotes, as suggested by monochromatic patches of regenerated crypts/villi illustrated in RFP (*H*), GFP (*I*), CFP (*J*), and YFP (*K*). *Insets* represent serial cross-sections through lineage traces indicating involvement of multiple contiguous crypts and villi (*G* and *K*).

at baseline but actively contribute to injury-associated repair upon quantitative loss of the Lgr5$^+$ population or crypt injury and suggest that Bmi1$^+$ ISCs play a larger role during epithelial repair than during basal homeostasis.

Isolated Bmi1$^+$ ISCs Are Multipotent and Give Rise to Lgr5-Expressing Cells in Vitro. Single Lgr5-eGFP$^+$ ISCs can generate in vitro spheroids in clonogenic culture without requiring a mesenchymal niche (19, 20). To determine whether Bmi1$^+$ ISCs can also form in vitro spheroids, we FACS-isolated single YFP$^+$ small intestine epithelial cells, representing Bmi1$^+$ ISCs, from 1 or 2 d tamoxifen-treated Bmi1-CreER; Rosa26-YFP mice. These purified single Bmi1-YFP$^+$ cells generated spheroids with similar morphology to Lgr5-eGFP-derived spheroids upon clonogenic culture in Matrigel with previously reported exogenous factors including Epidermal Growth Factor, Noggin, Jagged and Rspo1 (19) (Fig. 4 *A–D* and *I* and Fig. S3). Consistent with their in vivo stem cell function, the clonogenic spheroids grown from isolated Bmi1-YFP$^+$ single cells exhibited multipotency (Fig. 4 *E–H*), continued proliferation (Fig. 4*J*), and maintenance of pan-YFP expression upon serial passage (>8 mo with weekly passages) (Fig. S3). Notably, numerous Lgr5$^+$ cells were detected by Lgr5 mRNA fluorescence in situ hybridization (FISH) within the Bmi1$^+$ clonally derived spheroids (Fig. 4*K* and Fig. S4), whose clonogenicity was confirmed by the genetic signature of pan-YFP expression seen by both intrinsic YFP fluorescence and immunodetection (Fig. 4 *D* and *K*), indicating that the Bmi1$^+$ ISC lineage can generate Lgr5$^+$ cells in vitro.

Discussion

Our findings reveal that under both homeostatic and injury-induced conditions, Bmi1 and Lgr5 mark functionally distinct ISC populations in vivo. Although Lgr5$^+$ ISCs are extremely sensitive to Rspo1-mediated Wnt stimulation and Dkk1-mediated Wnt inhibition, Bmi1$^+$ ISCs are relatively refractory to Wnt manipulation. Further, although Lgr5$^+$ ISCs are actively cycling and quantitatively ablated by irradiation injury, the normally quiescent Bmi1$^+$ ISCs are instead induced to proliferate upon irradiation and, in fact, give rise to progeny that clonally repopulate multiple contiguous crypt-villus axes during subsequent intestinal regeneration.

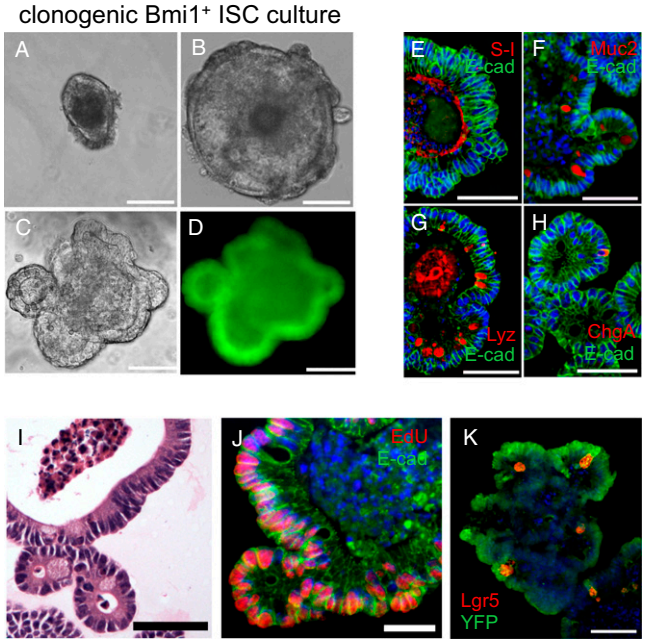

Fig. 4. Clonogenic culture of single FACS-isolated Bmi1-YFP$^+$ ISCs. (*A–D*) Single sorted Bmi1-YFP$^+$ cells marked by 1 or 2 d tamoxifen administration in Bmi1-CreER; Rosa-YFP mice form intestinal epithelial spheroids in clonogenic culture that demonstrate continued proliferation and self-renewal. Bright-field images of spheroids by 3 (*A*), 10 (*B*), and 14 d (*C*) in culture with pan-YFP expression visualized by direct fluorescence (*D*), consistent with clonal-derivation from a genetically marked Bmi1-expressing cell. (*E–H*) Bmi1-YFP$^+$ ISCs are multipotent in vitro by immunofluorescence antibody detection of lineage markers within clonogenic spheroids including sucrase-isomaltase for enterocytes (*E*), Muc2 for goblet cells (*F*), lysozyme for Paneth cells (*G*), and chromogranin A for enteroendocrine cells (*H*). E-cadherin is colored green and DAPI blue. (*I*) H&E staining of Bmi1-YFP$^+$ spheroid. (*J*) Proliferation of Bmi1-YFP$^+$ spheroid by EdU incorporation. E-cadherin is colored green and DAPI blue. (*K*) Clonogenically cultured Bmi1-YFP$^+$ spheroid from FACS-isolated single cells gives rise to multiple Lgr5$^+$ cells in vitro by Lgr5 FISH. Simultaneous Lgr5 FISH was performed with immunodetection of YFP, demonstrating that Lgr5$^+$ cells are clonally derived from a cell genetically marked with YFP expression in a Bmi1-CreER; Rosa-YFP mouse. DAPI is shown in blue. (Scale bars: *A–D*, 100 μm; *E–I* and *K*, 50 μm; *J*, 25 μm.)

Our results thus provide direct evidence that Bmi1$^+$ ISCs represent a quiescent, injury-inducible reserve ISC population, consistent with a proposed model for coexistence of distinct ISCs active during homeostasis vs. regeneration (10, 11, 21).

Tian and colleagues reported an elegant diphtheria toxin receptor (dTR) knock-in genetic strategy to selectively ablate Lgr5$^+$ ISCs in vivo using diphtheria toxin, revealing that Lgr5$^+$ ISCs are dispensable for intestinal homeostasis (9). Lgr5$^+$ ISC ablation was accompanied by expansion of the Bmi1$^+$ lineage, which is capable of giving rise to Lgr5-expressing cells in vivo (9). Their findings parallel and support our overall conclusions that the Bmi1$^+$ lineage expands upon quantitative loss of the Lgr5$^+$ population and of their lineage interrelationship. Notably, dTR-mediated genetic ablation of Lgr5$^+$ ISCs differs from our radiation injury model because of the lack of crypt loss observed upon diphtheria toxin ablation. Moreover, the mediation of epithelial reconstitution by Bmi1$^+$ ISCs after Lgr5$^+$ ISC ablation by either dTR or radiation injury does not distinguish between models in which these two populations are either functionally redundant or alternatively possess distinct functions. Our data, which reveal profound differences between Bmi1$^+$ and Lgr5$^+$ ISCs in baseline quiescence, cell-cycle entry after injury, effects of Wnt gain- and loss-of-function, and radiosensitivity, strongly argue for the latter model. The functional differences we describe therefore resolve the fundamental question of whether Bmi1$^+$ and Lgr5$^+$ ISCs are redundant or distinct populations and indicate that Bmi1$^+$ ISC recruitment after injury marks the utilization of a functionally discrete ISC class. Finally, our findings of Bmi1$^+$ ISC baseline quiescence and inducible proliferation after crypt injury provide functional evidence for Bmi1$^+$ ISC as a postulated injury-mobilized population and further underscore the heterogeneity of ISC populations contributing to tissue regeneration.

It is certainly possible that Bmi1 may only mark a subset of quiescent stem cells, and our results do not exclude overlapping expression with populations identified by other putative ISC molecular markers (8, 22–31), including those that may also function as quiescent and injury-mobilized ISCs. Additional proliferating cells not marked by Bmi1 are present in 2-d post-irradiated crypts using our tamoxifen-labeling strategy, suggesting either variegated Bmi1 expression in our reporter system or the contribution of other ISC populations to regeneration that perhaps also mediate postinjury regional repair of the colon and distal small intestine. The relative scarcity of Bmi1$^+$ ISCs may be insufficient to repair the entire intestinal epithelium after irradiation, and Bmi1$^+$ ISC are not present in colon (2, 9). Other ISCs markers have been proposed for identification of +4 position quiescent cells including Dcamkl1 (28), mTert (8), and Hopx (32), and these cells themselves may exhibit heterogeneity because there are numerous cells occupying this crypt position within the annulus of the 3D crypt. Notably, mTert has been described to mark an ISC population at the +4 position mobilized after radiation injury, and which overlaps in expression with both Lgr5 and Bmi1 (8, 33). Certainly, the potential overlap or interrelatedness of Bmi1$^+$ and mTert$^+$ ISCs and other +4 position markers such as Dcamkl1 and Hopx warrants further investigation. Further, the significance of overlapping Lgr5 coexpression within Bmi1$^+$ ISCs (9) and the proportion of Bmi1 mRNA-positive cells that are labeled by Bmi1-CreER remain to be determined.

Clonogenic cultures derived from isolated single Bmi1-YFP$^+$ cells give rise to all differentiated intestinal lineages and Lgr5$^+$ cells, supporting a lineage relationship where a quiescent ISC can give rise to an actively cycling ISC, and parallels in vivo observations of Lgr5$^+$ cell generation from Bmi1$^+$ ISCs (9). This work demonstrates clonogenic culture of the Bmi1$^+$ ISC population. Intriguingly, upon removal from the native tissue microenvironment and FACS isolation, the normally quiescent Bmi1$^+$ ISCs generate clonally derived intestinal spheroids with similar kinetics, morphology, and histology to those derived from single Lgr5$^+$ ISCs (19). The self-renewal and proliferation of the Bmi1-derived spheroids, like those derived from Lgr5, are Rspo1-dependent, consistent with prior results with Bmi1$^+$ lineage tracing in air-liquid interface organotypic cultures (17), whereas Bmi1$^+$ ISCs are relatively insensitive to Rspo1-Fc in vivo. These results are potentially consistent with a model where Bmi1$^+$ ISC are subject to considerable in vivo repression within the ISC niche, which does not appear to be recapitulated by current in vitro culture systems. Further, the clonogenic culture conditions used here, which were initially reported for Lgr5$^+$ ISCs (19), may actually select for an actively cycling state. Despite their functional differences in vivo, we cannot completely exclude potential concomitant overlapping Lgr5 coexpression within Bmi1$^+$ ISCs. It also remains to be determined whether the observed differences between the in vivo and in vitro properties are cell autonomous or due to differences in stem cell niche interactions.

Isolated Bmi1$^+$ ISCs can give rise to Lgr5$^+$ cells in vitro, and in vivo under homeostasis or dTR-mediated Lgr5$^+$ cell ablation (9), although the frequency of this occurrence is unknown. This lineage could occur infrequently during homeostasis in vivo, given the relative paucity of Bmi1$^+$ lineage contribution to basal regeneration. This lineage relationship could possibly also be bidirectional with Lgr5$^+$ ISCs giving rise to Bmi1$^+$ ISCs, paralleling the Lgr5/Hopx bidirectional relationship (32), with superimposed regulatory mechanisms to control the total number of ISCs, to regulate the balance of active and quiescent ISCs within the total stem cell pool, and to restrain homeostatic Bmi1$^+$ ISC proliferation. Overall, our findings of multiple functional distinctions between Bmi1$^+$ and Lgr5$^+$ ISCs provide direct evidence to support a proposed model of separate but cooperative functional roles of multiple and distinct ISC populations (10, 11, 21) residing in adjacent niches that contribute to homeostatic vs. injury-induced regeneration, with Bmi1$^+$ ISCs representing a quiescent, injury-inducible reserve ISC population. Further, the demonstration of Bmi1$^+$ ISCs giving rise to Lgr5-expressing cells underscores the potentially complex interplay between these two populations.

Materials and Methods

Lgr5-eGFP-IRES-CreERT2 mice were crossed with Rosa26-TdTomato or Rosa26-YFP to generate Lgr5-eGFP-IRES-CreERT2; Rosa26-TdTomato or Lgr5-eGFP-IRES-CreERT2; Rosa26-YFP compound heterozygotes, respectively. Likewise, Bmi1-CreER mice were crossed to Rosa26-YFP or Rosa26-Confetti to generate Bmi1-CreER; Rosa26-YFP or Bmi1-CreER; Rosa26-Confetti compound heterozygotes, respectively. Adult mice were injected with i.p. tamoxifen (Sigma) (9 mg per 40 g of body weight) to label Bmi1 ISCs and Bmi1$^+$ and Lgr5$^+$ lineages. For adenovirus-mediated modulation of Wnt signaling, 5×10^8 p.f.u. of Ad Fc, Ad Rspo1-Fc, or Ad Dkk1 was injected (i.v.) per mouse. For irradiation injury studies, mice were given 12 Gy whole-body irradiation and tissue was harvested at multiple time points after irradiation injury. For proliferation studies, 1 mg of EdU (Invitrogen) was injected (i.p.) 4 h before killing and EdU incorporation was evaluated according to the manufacturer's instructions with the Click-iT EdU Imaging Kit (Invitrogen) on OCT (Tissue-Tek) frozen sections. FACS experiments were performed with fresh small intestine epithelial preparations isolated with 10 mM EDTA chelation and enzymatic dissociation with collagenase/dispase (34) (Roche). For Bmi1-derived clonogenic cultures, 2- to 3-wk-old Bmi1-CreER; Rosa26-YFP mice were treated with tamoxifen as above. Tissue was dissociated into single cells for FACS isolation. Antibody staining was performed with anti-CD45, anti-CD31, and anti-EpCAM antibodies (eBioscience). CD31$^-$ CD45$^-$ EpCAM$^+$ YFP$^+$ single cells were isolated by FACS and clonogenically cultured as described (19). FISH was performed on 6-μm paraffin-embedded Bmi1-derived clonogenic spheroids by using Lgr5 digoxigenin-labeled probes as described (17), with simultaneous immunodetection of YFP using anti-GFP antibody (Aves).

ACKNOWLEDGMENTS. We thank members of the C.J.K. laboratory, Cecile Chartier, Michael Helmrath and Jill Carrington for discussions; Hans Clevers for Rosa26-Confetti mice; Anson Lowe for anti-sucrase-isomaltase anti-

body; and Scott Magness and Susan Henning for guidance in epithelial dissociation and clonogenic culture methods. K.S.Y. is an MD Scholar of the California Institute for Regenerative Medicine (CIRM) and also funded by a T32 Gastroenterology Training Grant at Stanford University. L.A.C. was supported by National Institutes of Health (NIH) F31 Fellowship and X.L. by a Stanford University Dean's Fellowship. E.S. was funded by Associazione Italiana per la Ricerca sul Cancro Grant MFAG 9141. These studies were funded by NIH Grant 1U01DK085527-01 as part of the NIH Intestinal Stem Cell Consortium supported by the National Institute of Diabetes and Digestive and Kidney Diseases and National Institute of Allergy and Infectious Diseases Grants 1R01DK085720-01 and 1R01 DK069989-01; CIRM Grant RS1-00243-1, the Digestive Diseases Center at Stanford University, and the Broad Medical Research Program of The Broad Foundation (to C.J.K.).

1. Barker N, et al. (2007) Identification of stem cells in small intestine and colon by marker gene Lgr5. *Nature* 449:1003–1007.
2. Sangiorgi E, Capecchi MR (2008) Bmi1 is expressed in vivo in intestinal stem cells. *Nat Genet* 40:915–920.
3. Cheng H, Leblond CP (1974) Origin, differentiation and renewal of the four main epithelial cell types in the mouse small intestine. V. Unitarian Theory of the origin of the four epithelial cell types. *Am J Anat* 141:537–561.
4. Snippert HJ, et al. (2010) Intestinal crypt homeostasis results from neutral competition between symmetrically dividing Lgr5 stem cells. *Cell* 143:134–144.
5. Simons BD, Clevers H (2011) Strategies for homeostatic stem cell self-renewal in adult tissues. *Cell* 145:851–862.
6. Lopez-Garcia C, Klein AM, Simons BD, Winton DJ (2010) Intestinal stem cell replacement follows a pattern of neutral drift. *Science* 330:822–825.
7. van der Flier LG, et al. (2009) Transcription factor achaete scute-like 2 controls intestinal stem cell fate. *Cell* 136:903–912.
8. Montgomery RK, et al. (2011) Mouse telomerase reverse transcriptase (mTert) expression marks slowly cycling intestinal stem cells. *Proc Natl Acad Sci USA* 108: 179–184.
9. Tian H, et al. (2011) A reserve stem cell population in small intestine renders Lgr5-positive cells dispensable. *Nature* 478:255–260.
10. Li L, Clevers H (2010) Coexistence of quiescent and active adult stem cells in mammals. *Science* 327:542–545.
11. Greco V, Guo S (2010) Compartmentalized organization: A common and required feature of stem cell niches? *Development* 137:1586–1594.
12. Potten CS, Kovacs L, Hamilton E (1974) Continuous labelling studies on mouse skin and intestine. *Cell Tissue Kinet* 7:271–283.
13. Potten CS, Owen G, Booth D (2002) Intestinal stem cells protect their genome by selective segregation of template DNA strands. *J Cell Sci* 115:2381–2388.
14. Kuhnert F, et al. (2004) Essential requirement for Wnt signaling in proliferation of adult small intestine and colon revealed by adenoviral expression of Dickkopf-1. *Proc Natl Acad Sci USA* 101:266–271.
15. Pinto D, Gregorieff A, Begthel H, Clevers H (2003) Canonical Wnt signals are essential for homeostasis of the intestinal epithelium. *Genes Dev* 17:1709–1713.
16. Muncan V, et al. (2006) Rapid loss of intestinal crypts upon conditional deletion of the Wnt/Tcf-4 target gene c-Myc. *Mol Cell Biol* 26:8418–8426.
17. Ootani A, et al. (2009) Sustained in vitro intestinal epithelial culture within a Wnt-dependent stem cell niche. *Nat Med* 15:701–706.
18. Kim KA, et al. (2005) Mitogenic influence of human R-spondin1 on the intestinal epithelium. *Science* 309:1256–1259.
19. Sato T, et al. (2009) Single Lgr5 stem cells build crypt-villus structures in vitro without a mesenchymal niche. *Nature* 459:262–265.
20. Sato T, et al. (2011) Paneth cells constitute the niche for Lgr5 stem cells in intestinal crypts. *Nature* 469:415–418.
21. Scoville DH, Sato T, He XC, Li L (2008) Current view: Intestinal stem cells and signaling. *Gastroenterology* 134:849–864.
22. Potten CS, et al. (2003) Identification of a putative intestinal stem cell and early lineage marker; musashi-1. *Differentiation* 71:28–41.
23. He XC, et al. (2004) BMP signaling inhibits intestinal stem cell self-renewal through suppression of Wnt-beta-catenin signaling. *Nat Genet* 36:1117–1121.
24. He XC, et al. (2007) PTEN-deficient intestinal stem cells initiate intestinal polyposis. *Nat Genet* 39:189–198.
25. Zhu L, et al. (2009) Prominin 1 marks intestinal stem cells that are susceptible to neoplastic transformation. *Nature* 457:603–607.
26. Formeister EJ, et al. (2009) Distinct SOX9 levels differentially mark stem/progenitor populations and enteroendocrine cells of the small intestine epithelium. *Am J Physiol Gastrointest Liver Physiol* 296:G1108–G1118.
27. May R, et al. (2008) Identification of a novel putative gastrointestinal stem cell and adenoma stem cell marker, doublecortin and CaM kinase-like-1, following radiation injury and in adenomatous polyposis coli/multiple intestinal neoplasia mice. *Stem Cells* 26:630–637.
28. May R, et al. (2009) Doublecortin and CaM kinase-like-1 and leucine-rich-repeat-containing G-protein-coupled receptor mark quiescent and cycling intestinal stem cells, respectively. *Stem Cells* 27:2571–2579.
29. Levin TG, et al. (2010) Characterization of the intestinal cancer stem cell marker CD166 in the human and mouse gastrointestinal tract. *Gastroenterology* 139:2072–2082, e2075.
30. von Furstenberg RJ, et al. (2011) Sorting mouse jejunal epithelial cells with CD24 yields a population with characteristics of intestinal stem cells. *Am J Physiol Gastrointest Liver Physiol* 300:G409–G417.
31. Furuyama K, et al. (2011) Continuous cell supply from a Sox9-expressing progenitor zone in adult liver, exocrine pancreas and intestine. *Nat Genet* 43:34–41.
32. Takeda N, et al. (November 10, 2011) Interconversion between intestinal stem cell populations in distinct niches. *Science,* 10.1126/science.1213214.
33. Schepers AG, Vries R, van den Born M, van de Wetering M, Clevers H (2011) Lgr5 intestinal stem cells have high telomerase activity and randomly segregate their chromosomes. *EMBO J* 30:1104–1109.
34. Gracz AD, Ramalingam S, Magness ST (2010) Sox9 expression marks a subset of CD24-expressing small intestine epithelial stem cells that form organoids in vitro. *Am J Physiol Gastrointest Liver Physiol* 298:G590–G600.